



HAL
open science

Role of ATP-hydrolysis in the dynamics of a single actin filament

Padinhateeri Ranjith, Kirone Mallick, Jean-François Joanny, David Lacoste

► To cite this version:

Padinhateeri Ranjith, Kirone Mallick, Jean-François Joanny, David Lacoste. Role of ATP-hydrolysis in the dynamics of a single actin filament. *Biophysical Journal*, 2010, 98 (8), pp.1418-1427. 10.1016/j.bpj.2009.12.4306 . cea-02924677

HAL Id: cea-02924677

<https://cea.hal.science/cea-02924677v1>

Submitted on 28 Aug 2020

HAL is a multi-disciplinary open access archive for the deposit and dissemination of scientific research documents, whether they are published or not. The documents may come from teaching and research institutions in France or abroad, or from public or private research centers.

L'archive ouverte pluridisciplinaire **HAL**, est destinée au dépôt et à la diffusion de documents scientifiques de niveau recherche, publiés ou non, émanant des établissements d'enseignement et de recherche français ou étrangers, des laboratoires publics ou privés.

Role of ATP-hydrolysis in the dynamics of a single actin filament

Padinhateeri Ranjith
Physico-Chimie UMR 168
Institut Curie, 26 rue d'Ulm
75248 Paris Cedex 05, France

Kirone Mallick
Service de Physique Théorique
CEA Saclay
91191 Gif, France

Jean-François Joanny
Physico-Chimie UMR 168
Institut Curie, 26 rue d'Ulm
75248 Paris Cedex 05, France

David Lacoste
Laboratoire de Physico-Chimie Théorique,
ESPCI, 10 rue Vauquelin,
Paris Cedex 05, France

Abstract

We study the stochastic dynamics of growth and shrinkage of single actin filaments taking into account insertion, removal, and ATP hydrolysis of subunits either according to the vectorial mechanism or to the random mechanism. In a previous work, we developed a model for a single actin or microtubule filament where hydrolysis occurred according to the vectorial mechanism: the filament could grow only from one end, and was in contact with a reservoir of monomers. Here we extend this approach in several ways, by including the dynamics of both ends and by comparing two possible mechanisms of ATP hydrolysis. Our emphasis is mainly on two possible limiting models for the mechanism of hydrolysis within a single filament, namely the vectorial or the random model. We propose a set of experiments to test the nature of the precise mechanism of hydrolysis within actin filaments.

Key words: Actin; ATP hydrolysis; Stochastic dynamics

Introduction

Actin monomers polymerize to form long helical filaments, by addition of monomers at the ends of the filament. The two ends are structurally different. The addition and removal of subunits at one end, the barbed end, are substantially faster than at the other end, the pointed end. In an equilibrium polymer, the critical concentration at which the on- and off-rates are balanced must be the same at both ends for thermodynamic reasons (1). But actin is not an equilibrium polymer, it is an ATPase, and ATP is rapidly hydrolyzed after polymerization. Due to this constant energy consumption, the actin polymer exhibits many interesting non-equilibrium features; most notably it is able to maintain different critical concentrations at the two ends (2). This allows the existence of a special steady-state called treadmilling, characterized by a flux of subunits going through the filament, which has been observed both with actin as well as with microtubules filaments (3).

The precise molecular mechanism of hydrolysis in actin has been controversial for many years. For each of the two steps involved in the hydrolysis (the ATP cleavage and the Pi release), the possibility of the reaction occurring either at the interface between neighboring units carrying different nucleotides or at random location within the filament can be invoked. The vectorial model corresponds to a limit of infinite cooperativity in which the hydrolysis of a given monomer depends entirely on the state of its neighbors, and the random model is a model of zero cooperativity in which the hydrolysis of a given monomer is independent of the state of its neighbors. In between these two limits, models with a finite cooperativity have been considered (4, 5). A direct evidence for a cooperative mechanism was brought recently by the authors of Ref. (6), who observed GTP-tubulin remnants using a specific antibody.

Several groups have emphasized the process of random cleavage followed by random Pi release (7, 8). By studying the polymerization of actin in the presence of phosphate, the authors of Ref. (2) argued that the crucial step of release of the phosphate is not a simple vectorial process but is probably cooperative. Since this release of phosphate is slow, the delay between the completion of hydrolysis and the polymerization can lead to overshoots which indeed have been observed in fluorescence intensity measurements of pyrene-labelled actin during rapid polymerization as discussed in (9). At the single filament level, the dynamics of depolymerization is also very interesting. The study of this dynamics provides insights into the underlying mechanism of hydrolysis in actin as discussed recently in Refs. (5, 10).

Although decades of work in the biochemistry of actin have provided a

lot of details on the kinetics of self-assembly of actin in the absence and in the presence of actin binding proteins, it is difficult to capture the complexity of this process without a mathematical model to organize all this information. To this end, we have studied a non-equilibrium model for a single actin or microtubule filament (11) based on the work of Stukalin et al. (12). In this model, the hydrolysis of subunits inside the filament is a vectorial process, the filament is in contact with a reservoir of monomers, and growth occurs only from one end. We have analyzed the phase diagram of that model with a special emphasis on the bounded growth phase, and we have discussed some features of the dynamic instability. Our approach differs from previous work on the dynamic instability of microtubules in the following way: the model is formulated in terms of rates associated with monomer addition/removal and hydrolysis rather than in terms of phenomenological parameters such as the switching rates between states of growth and collapse as done in Refs. (13, 14). This should be a definite advantage when bridging the gap between the theoretical model and experiments.

The work of Flyvbjerg et al. (14) has inspired a number of other theoretical models, based on a microscopic treatment of growth, decay, catastrophe and rescue of the filament: see in particular Ref. (15) and Refs. (16–18), which analyze using analytical and numerical methods several aspects of the dynamic instability of microtubules.

In this paper, we present a model for a single actin filament which accounts for the insertion, removal, and ATP hydrolysis of subunits at both ends. It extends our previous work (11) in several ways: first by including the dynamics of both ends and secondly by carrying out simulations for both mechanisms of hydrolysis – vectorial and random. In section 1 we present the first extension due to the inclusion of both ends, and in section 2 we study the two versions of the model for the hydrolysis within the filament. In the last section 3, we examine transient properties of a single filament using numerical simulations and we show that for these transient properties, the vectorial and random models lead to distinct behaviors. This suggests experiments that would allow to discriminate between the two models.

1 Vectorial model of hydrolysis with activity at both ends

ATP hydrolysis is a two steps process: the first step is the ATP cleavage which produces ADP-Pi, and which is rapid. The second step is the release of the phosphate (Pi), which leads to ADP-actin and which is by compar-

ison much slower (19). ADP-Pi-actin and ATP-actin have similar critical concentrations but they are kinetically different species, since they have different on and off rates as shown in Ref. (2). Nevertheless, from a kinetic point of view, the slow step of release of the phosphate is the rate-limiting essential step. This suggests that many kinetic features of actin polymerization can be explained by a simplified model of hydrolysis, which takes into account only the second step of hydrolysis and treats actin subunits bound to ATP and actin subunits bound to ADP-Pi as a single specie. This is the assumption of Ref. (12), which we have used in our published study (11) as well as in the present work. In other words, what is meant by hydrolysis in all these references is the step of Pi release. In this section, we assume that this release of Pi is a vectorial process described as a single reaction with rate R .

Let us recall the main features of the phase diagram of our previous model which assumes that only one end is growing. The model has three different phases: two phases of unbounded growth and one phase of bounded growth. In one phase of unbounded growth (phase III), both the cap and the bulk of the filament are unbounded. In this rapidly growing phase, the filament is essentially made of unhydrolyzed ATP-actin monomers. In the intermediate phase of unbounded growth (phase II), the cap length remains constant as a function of time while the length of the filament grows linearly with time. Finally, in the phase of bounded growth (phase I), both cap length and filament length remain constant on average. This phase is characterized by a finite average length $\langle l \rangle$ and by a specific length distribution of the filament which were calculated in Ref. (11). The phase of unbounded growth is frequently observed with actin, whereas the intermediate phase only exists as a steady state in a small interval of concentration of actin monomers near the critical concentration. The intermediate phase can, however, be observed outside this interval in a transient way, by forcing filaments to depolymerize through a dilution of the external medium. The phase of bounded growth of a single filament growing from one end only has not been observed experimentally so far with actin, but it has been observed and is well known in microtubules (13, 14).

We now extend the single-end model by including dynamics at both the ends. We keep, as before, the assumption of vectorial hydrolysis, which means that there is a single interface between the ATP subunit and ADP subunits, and the assumption of a reservoir of free ATP subunits in contact with the filament. The addition of ATP subunits occurs with rate U at the barbed end, the removal of ATP subunits occurs with rate W_T^+ at the barbed end and with a rate W_T^- at the pointed end. The removal of ADP

subunits occurs at the barbed end only if the cap is zero, with rate W_D^+ . At the pointed end, ADP subunits are removed with a rate W_D^- . Note that we neglect the possibility of addition of ATP subunits at the pointed end, this assumption is not essential but simplifies the analysis.

In Fig. 1, we have pictorially depicted all these moves discussed above. Furthermore, we have assumed that all the rates are independent of the concentration of free ATP subunits C except for the on-rate which is $U = k_0 C$. All the rates of this model have been determined precisely experimentally except for R . The values of these rates are given in table 1.

The state of the filament can be represented in terms of n , the number of ADP subunits and k the number of ATP subunits. The dynamics of the filament can be mapped onto that of a random walker in the upper-quarter plane (n, k) with the specific moves as shown in figure 1. We find the following steady-state phases (see Appendix A for details): a phase of bounded growth (phase I), and three phases of unbounded growth (phase IIA and IIB, phase III). The phase of bounded growth (phases I) and the phase of unbounded growth with unbounded cap (phase III) are similar to the corresponding phases in Ref. (11). In the phase IIA, similar to the phase II of that reference, the filament is growing linearly in time, with a velocity v_{IIA} but the average cap length remains constant in time. In the new phase IIB, the filament is growing linearly in time, with a velocity v_{IIB} but there is a section of ADP subunits which remains constant in time near the pointed end (this is analogous to the cap of ATP subunits near the barbed end in phase IIA).

This phase diagram can be understood from the random walk representation of figure 1. The velocity of the random walker in the bulk has components $v_n = (R - W_D^-)d$ along the x axis and $v_k = (U - W_T^+ - R)d$ along the y axis, where d is the subunit size. Depending on the signs of these quantities, four cases emerge. If $v_n > 0$ and $v_k > 0$, both the filament and cap length increase without bound, this corresponds to phase III. If $v_n < 0$ and $v_k < 0$, both the filament and cap length stay bounded and we have phase I. If $v_n > 0$ and $v_k < 0$, the cap length remains constant in time, but the rest of the filament made of D subunits can be either bounded (then we are again in phase I) or unbounded (and we are in phase IIA). Similarly, if $v_n < 0$ and $v_k > 0$, the length of the region of D subunits at the pointed end remain constant in time, but the region of T subunits can be either bounded (phase I) or unbounded (phase IIB). In phase IIA, the probability of finding a non-zero cap,

$$q = \frac{U}{W_T^+ + R}, \quad (1)$$

is finite, and the average filament velocity is (see Appendix A)

$$v_{IIA} = [U - W_T^+ q - W_D^+(1 - q) - W_D^-]d. \quad (2)$$

At the critical concentration $c = c_A$, $v_{IIA} = 0$ and this marks the boundary to phase I. We find that

$$c_A = \frac{(W_D^+ + W_D^-)}{k_0} \left(\frac{W_T^+ + R}{W_D^+ + R} \right), \quad (3)$$

which is always larger than the critical concentration of the barbed end alone. In region III, the velocity is still given by

$$v_{III} = [U - W_T^+]d. \quad (4)$$

Similarly, in phase IIB, the probability of finding a non-zero region of D-subunits $\tilde{q} = R/W_D^-$ is finite, and the average filament velocity is

$$v_{IIB} = [U - W_T^+ - W_T^-(1 - \tilde{q}) - W_D^-\tilde{q}]d, \quad (5)$$

which vanishes when $c = c_B$ at the boundary with phase I, with

$$c_B = \frac{1}{k_0} \left[(W_T^- - W_D^-) \left(1 - \frac{R}{W_D^-} \right) + (W_T^+ + W_D^-) \right]. \quad (6)$$

Note that W_T^- does not enter in v_{IIA} since the hydrolyzed part of the filament is always infinitely large in this case, in contrast to the case of v_{IIB} , which depends on both W_T^- and W_D^- . Note also that the velocity v_{IIA} and v_{IIB} are sums of a contribution due to the barbed end and a contribution due to the pointed end. This is due to the fact that in all growing phases, the filament is infinitely long in the steady state, and therefore the dynamics of each end is independent of the other.

Length fluctuations of the filament are characterized by a diffusion coefficient which is defined in Appendix A. Since the dynamics of each end is independent in phase IIA, the diffusion coefficient of this phase D_{IIA} is the sum of a contribution from the barbed end and another from the pointed end. From Ref.(11) we obtain,

$$D_{IIA} = \frac{d^2}{2} \left[U + W_T^+ q + W_D^+(1 - q) + \frac{2(W_D^+ - W_T^+)(U + W_D^+ q)}{W_T^+ + R} + W_D^- \right]. \quad (7)$$

where $(W_D^- d^2)/2$ is contribution of the diffusion coefficient due to the pointed end.

On the boundary lines $c = c_A$ and $c = c_B$, the average filament velocity vanishes. At this point, the addition of subunits at the barbed end exactly compensates the loss of subunits at the pointed end. Such a state is well known in the literature as treadmilling (21). There, the length diverges as $-D_{IIA}/v_{IIA}$ near $c = c_A$ and similarly as $-D_{IIB}/v_{IIB}$ near $c = c_B$ as shown in figure 5, where D_{IIA} and D_{IIB} are diffusion coefficient in phases *IIA* and *IIB*. That divergence is a consequence of the assumption that the filament is in contact with a reservoir of monomers, in experimental conditions the maximum length is fixed by the total amount of monomers. In the bulk of phase I, the average velocity is zero due to a succession of collapses and nucleations of a new filament. In this phase, there is a steady state with a well-defined treadmilling average length.

As mentioned above, since the two ends are far from each other in the growing phases, they can be treated independently. In the phase of bounded growth (phase I) however, where the filament length reaches zero occasionally, the two ends are interacting strongly. For this reason, a precise description of the phase of bounded growth is more difficult (see Appendix A). Because of this, we have computed numerically the average length in Fig. 5 as function of the free monomer concentration. In this figure, we compare the case of the filament with two ends to the case with one end only. We see that there is a small increase in the critical concentration where the length diverges and a corresponding lowering of the average length due to the inclusion of both ends in the model. This effect is correctly captured by Eqs. 3-6. Note that although there are large length fluctuations in phase I, the diffusion coefficient D_I as defined in appendix A is zero in phase I, because these fluctuations do not depend on time.

2 Hydrolysis within the filament: a vectorial or random process ?

2.1 Growth velocity

As explained earlier, we have used a simplified model for hydrolysis (12), in which the first step of hydrolysis is absent. The only remaining step, the phosphate release, is assumed to be a vectorial process. In the following, we keep this assumption, but we compare the two limiting mechanisms for the phosphate release, namely the vectorial and the random processes. All the rates have the same meaning for both models, except for the hydrolysis rate which is denoted R in the vectorial model and r in the random model.

We have compared experimental data from (22) together with the two theoretical models, vectorial and random. Both models successfully account for the observed sharp bend in the velocity versus concentration plots observed near the critical concentration as shown in figure 7. Below the critical concentration, the velocity is negative for depolymerizing filaments and it is the velocity of phase II, since phase II extends transiently below the critical concentration.

Note that the velocities of both models superimpose, which means that bulk velocity measurements do not allow to discriminate between these models. Irrespective of the actual hydrolysis (phosphate release) mechanism, a fit of this data provides a bound on the value of the hydrolysis rate in the vectorial model R which is not accurately determined experimentally. This parameter, was roughly estimated in Ref.(12) to be $0.3s^{-1}$ based on measurements of Pi release by Melki et al. (23). The measured hydrolysis rate was multiplied by a typical length to get the estimate for R . Our fit of the data of Ref.(24), gives $R = 0.1 \pm 0.12s^{-1}$. This is the value which we have used for later comparison.

In figure 6, the phase diagram of the random hydrolysis model is shown. This phase diagram has only two phases in contrast to the vectorial case, because it can be shown that the average of the total amount of ATP subunits $\langle k \rangle$ is always bounded in the random model. Thus phase III is absent in the random model. In appendix B, we present details about the derivation of the mean-field equations for the random model (25, 26). An analytical expression for the phase boundary between phase I and II is obtained, which corresponds to the solid line in figure 6 and which agrees well with the Monte Carlo simulations.

2.2 Length diffusivity

Length fluctuations are quantified by the length diffusivity also called diffusion coefficient D which is defined in Eq. 18 of Appendix A. The length diffusivity of single filaments has been measured using TIRF microscopy by two groups (27, 28). Both groups reported rather high values, of the order of $30 \text{ monomer}^2/\text{s}$. This value is high when thinking in terms of the rates of assembly and disassembly measured in bulk (29, 30). From such bulk measurements, one could have expected a length diffusivity at the critical concentration of $1 \text{ monomer}^2/\text{s}$; so an order of magnitude smaller than observed in single filament experiments.

Several studies have been carried out to explain this discrepancy: Vavylonis et al. (7) computed the diffusion coefficient D as a function of ATP

monomer concentration and found that D is peaked just below the critical concentration and its maximum is comparable to the value observed in experiments (≈ 30 monomer²/s). Stukalin et al (12) obtained from an analytical model the same large values for D (≈ 30 monomer²/s) just above the critical concentration. Recently, Fass et al. studied the length diffusivity numerically taking into account filament fragmentation and annealing, within the vectorial model (20). They found that high length diffusivity at the critical concentration cannot be explained by fragmentation and annealing events unless both fragmentation and annealing rates are much greater than previously thought. In the limit where their fragmentation rate goes to zero, they recover the results of Ref. (7). Others have expressed the opinion that the discrepancy in diffusivity may be related to experimental errors in the length of the filament due to out of plane bending of the filaments (M. F. Carlier, private communication).

According to Stukalin et al (12) and Vavylonis et al (7), the large length diffusivity observed in experiments results from dynamic instability-like fluctuations of the cap. It is important to point out that both papers make very different assumptions: the first one describes hydrolysis as a single step corresponding to Pi release with the vectorial mechanism, whereas the second one describes both steps as random processes.

We have shown in figure 8 the concentration dependence of D for the vectorial model using analytical expressions provided in the appendix and similar to that of (11, 12). In this figure, the critical concentration defined as the boundary between phases I and II almost coincides with the concentration at the boundary between phases II and III, both are of the order of $0.14 \mu\text{M}$. Above this value, D is indeed small, the expected estimate of 1 monomer²/s is indeed recovered there because the contribution of hydrolysis is negligible. Near the critical concentration, however, the fluctuations are much larger, for a reason which is similar to the reason that leads to large fluctuations near critical points in condensed matter systems (31). Here, hydrolysis which is known to destabilize filaments, has a larger effect. It leads to large fluctuations of the cap, and ultimately to a large length diffusivity. Note that the region below the critical concentration corresponds to the transient extension of phase II discussed in the previous section. If the fluctuations were probed there for a very long time, one would find $D = D_I = 0$, characteristic of phase I.

In figure 8, we have compared these analytical results obtained for the vectorial model with numerical results obtained for the random model. In the random model, we use Monte Carlo simulations to calculate a time dependent diffusion coefficient $D(t)$, defined as $D(t) = \frac{1}{2} \frac{d}{dt} (\langle l^2 \rangle - \langle l \rangle^2)$. For

concentrations larger than the critical concentration, the initial condition is $l(t=0) = 0$, whereas for concentrations smaller than the critical concentration, the initial condition was a very long filament ($l(t=0) > 10^6$ subunits) with all subunits in the hydrolyzed state. On a large time window, we find that $D(t)$ is approximately time independent, and we interpret that value as the length diffusivity of the random model. Our results fully agree with that of Ref. (7), and with that of Ref. (20) in the limit of zero fragmentation rate. The length diffusivity indeed reaches a maximum of the order of 30 monomer²/s below the critical concentration. As shown in that figure, there is only a small difference of length diffusivity in the vectorial case as compared to the random case: the maximum of the curve for the random model occurs at a smaller concentration than in the vectorial model. The fact that we are able to reproduce a similar curve as in Refs. (7, 20) justifies our simplifying assumption of describing the hydrolysis as a single step associated with the release of phosphate rather than taking into account the two steps as done in these references. More importantly it confirms the idea that the length diffusivity of actin, near critical concentration, is dominated by a process similar to the dynamic instability, which is essentially captured by the vectorial model.

To make further progress, it would be very useful to reproduce experiments similar to those of Ref. (27), on single filaments for various monomer concentrations, to confirm the scenario presented above for the length fluctuations of actin. Given that the predictions of the random and vectorial model are rather close to each other as shown in our figure 8, it is likely that it will be difficult to distinguish between these models from measurements of the concentration dependence of the length diffusivity. One reason for which the length diffusivity of the two models are very close to each other is that a very small value of the hydrolysis rate r (as estimated from experiments) has been used, we have observed that if this parameter had a larger value than expected, the predictions of the vectorial and random model would differ much more.

3 Dynamics of the filament in transient regimes

Since it appears difficult to distinguish the vectorial from the random model using measurements of growth velocity or length diffusivity, one can turn to an analysis of the dynamics of the filament length in polymerization (27) or in depolymerization (5, 10) to discriminate between the two models. Here, we focus on the dynamics of polymerization of a single filament, in

the presence of a constraint of conservation of the total number of subunits (free+polymerized). This constraint leads to a steady state with a constant average length for the filament. We compare the time it takes for the filament to be fully hydrolyzed to the time that it takes to reach the steady state length. We also discuss the corresponding length fluctuations as a function of time. We argue that both measurements (the lag time of hydrolysis and the time resolved fluctuations) can distinguish between the two mechanisms of hydrolysis.

In Fig. 9 we show the filament length as well as its variance, as a function of time, for both vectorial and random models. Using Monte Carlo simulations we computed $l(t)$, starting from $l(t=0) = 0$, for 1000 different realizations and calculated $\sigma^2(t) = \langle l^2 \rangle - \langle l \rangle^2$. Concerning the lag time of hydrolysis, we have observed that in simulations of the vectorial model, the filament typically reaches its steady state length long before it has been completely hydrolyzed. The time when this happens corresponds to the point where the two curves meet in Fig. 9 (a). This characteristic time since only one end is involved, is $t_H \simeq \langle l \rangle / R$ where R is the hydrolysis rate in the vectorial model (11). From the figure we find that $t_H \simeq 3500/0.3 \simeq 11000\text{s} \simeq 180 \text{ min}$ (with $R \simeq 0.3$, which is much longer than the typical time to reach the steady state $t_{SS} \simeq \langle l \rangle / v \simeq 3500 / (11.6 \times 0.7 - 1.4) = 520\text{s}$). In contrast to this, in the random model, the time for completion of hydrolysis is comparable to the time to reach steady state (see Fig. 9 (b)) as both the filament and the ADP part have similar growth dynamics.

In practice, this lag time of hydrolysis may be difficult to measure on single filaments since the ATP subunits and ADP subunits can not be distinguished easily experimentally. In view of the previous section, on the role of ATP hydrolysis in length diffusivity, we suggest to study instead the length fluctuations of the filament as a function of time. Such a quantity is accessible from image analysis of single filaments with TIRF for instance. We have simulated the variance of the length fluctuations $\sigma(t)^2 = \langle l(t)^2 \rangle - \langle l(t) \rangle^2$ as function of time, for the vectorial model and random model, as shown in Fig. 9 (c) and (d) respectively. At early times, this variance is linear in time, and the slope corresponds to the length diffusivity discussed in previous section, because the constraint of conservation of monomers plays no role at short times. Once the steady state has been reached, we find that the variance of the vectorial model shows a sharp increase when $t \geq t_H$, while the variance of the random model shows no significant change. The approximately constant variance of the random model is intermediate between the variance of the vectorial model before and after the jump.

Thus contrary to velocity and length diffusivity measurements, an anal-

ysis of either the lag time of hydrolysis or of the time dependence of the length fluctuations provide a direct signature of the underlying mechanism of hydrolysis.

4 Conclusion

In this article, we have analyzed several aspects of the dynamics of a single actin filament. Many results discussed above could be extended *mutatis mutandis* to the case of microtubules.

We have constructed a phase diagram, which summarizes all the possible dynamical phases of an actin filament with two active ends and vectorial hydrolysis in its inside. We have found that quantities like the filament velocity and the length diffusivity show similar behavior for both vectorial and random model of hydrolysis. We propose that measuring the length fluctuations of a single filament as a function of time can distinguish between the two models for hydrolysis (or to be more precise to the step of phosphate release). Although more experimental and theoretical work are needed, studies of the dynamics of the length of single filaments during polymerization (27) and during depolymerization (5, 10) suggest a mechanism of phosphate release which is not purely vectorial or purely random, but rather partially cooperative.

We hope that our study will contribute to the understanding of the non-equilibrium self-assembly of actin/microtubule filaments.

4.1 Acknowledgements

We thank M. F. Carlier, J. Baudry, I. Fujiwara and A. Kolomeisky for illuminating discussions. We also acknowledge discussions with S. Sumedha, B. Chakraborty and F. Perez. We thank D. Blair for his contribution to the numerical study of the random model. We acknowledge support from the Indo-French Center CEFIPRA (grant No. 3504-2), and from Chaire Joliot (ESPCI).

Appendix

A Equations of the vectorial model with two ends

Let $P(n, k, t)$ be the probability of having n hydrolyzed ADP subunits and k unhydrolyzed ATP subunits at time t , such that $l = (n + k)d$ is the total length of the filament. It obeys the following master equation: For $k > 0$ and $n > 0$ we have

$$\begin{aligned} \frac{dP(n, k, t)}{dt} = & UP(n, k - 1, t) + W_T^+ P(n, k + 1, t) + RP(n - 1, k + 1, t) \\ & + W_D^- P(n + 1, k) - (U + W_T^+ + R + W_D^-) P(n, k, t). \end{aligned} \quad (8)$$

For $k > 0$ and $n = 0$

$$\begin{aligned} \frac{dP(0, k, t)}{dt} = & UP(0, k - 1, t) + (W_T^+ + W_T^-) P(0, k + 1, t) \\ & + W_D^- P(1, k) - (U + W_T^+ + W_T^- + R) P(0, k, t). \end{aligned} \quad (9)$$

For $k = 0$ and $n \geq 1$ we have,

$$\frac{dP(n, 0, t)}{dt} = (W_D^+ + W_D^-) P(n + 1, 0, t) + W_T^+ P(n, 1, t) + RP(n - 1, 1, t) - (U + W_D^+ + W_D^-) P(n, 0, t). \quad (10)$$

If $k = 0$ and $n = 0$, we have

$$\frac{dP(0, 0, t)}{dt} = (W_T^+ + W_T^-) P(0, 1, t) + (W_D^+ + W_D^-) P(1, 0, t) - UP(0, 0, t). \quad (11)$$

We define the following generating functions

$$G(x, y, t) = \sum_{n \geq 0} \sum_{k \geq 0} P(n, k, t) x^n y^k, \quad (12)$$

$$F_k(x, t) = \sum_{n \geq 0} P(n, k, t) x^n, \quad (13)$$

$$H_n(y, t) = \sum_{k \geq 0} P(n, k, t) y^k. \quad (14)$$

Normalization imposes that at all times t ,

$$G(1, 1, t) = \sum_{n=0}^{\infty} \sum_{k=0}^{\infty} P(n, k, t) = 1. \quad (15)$$

Using eqs 8, 9, 10 and 11, we obtain the evolution equation for $G(x, y, t)$

$$\begin{aligned}
\frac{dG(x, y, t)}{dt} &= \left[U(y-1) + W_T^+ \left(\frac{1}{y} - 1 \right) + R \left(\frac{x}{y} - 1 \right) + W_D^- \left(\frac{1}{x} - 1 \right) \right] G(x, y, t) \\
&- \left[W_T^+ \left(\frac{1}{y} - 1 \right) + R \left(\frac{x}{y} - 1 \right) + W_D^+ \left(1 - \frac{1}{x} \right) \right] F_0(x, t) \\
&- \left[W_D^- \left(\frac{1}{x} - 1 \right) + W_T^- \left(1 - \frac{1}{y} \right) \right] H_0(y, t) \\
&- \left[W_D^+ \left(\frac{1}{x} - 1 \right) - W_T^- \left(1 - \frac{1}{y} \right) \right] P(0, 0, t).
\end{aligned} \tag{16}$$

From $G(x, y, t)$, the following quantities can be obtained: the velocity of the filament, which is

$$v = \lim_{t \rightarrow \infty} \frac{d\langle l \rangle}{dt} = d \lim_{t \rightarrow \infty} \frac{\partial}{\partial x} \left(\frac{dG(x, x, t)}{dt} \right)_{x=1}, \tag{17}$$

the diffusion coefficient characterizing filament length fluctuations

$$\begin{aligned}
D &= \lim_{t \rightarrow \infty} \frac{1}{2} \frac{d}{dt} (\langle l^2 \rangle - \langle l \rangle^2) \\
&= d^2 \lim_{t \rightarrow \infty} \left[\frac{1}{2} \frac{\partial^2}{\partial x^2} \left(\frac{dG(x, x, t)}{dt} \right) + \frac{1}{2} \frac{\partial}{\partial x} \left(\frac{dG(x, x, t)}{dt} \right) \right. \\
&\quad \left. - \left(\frac{\partial G(x, x, t)}{\partial x} \right) \frac{\partial}{\partial x} \left(\frac{dG(x, x, t)}{dt} \right) \right]_{x=1}.
\end{aligned} \tag{18}$$

The average cap velocity is

$$J = d \lim_{t \rightarrow \infty} \frac{d\langle k \rangle}{dt} = d \lim_{t \rightarrow \infty} \frac{\partial}{\partial y} \left(\frac{dG(1, y, t)}{dt} \right)_{y=1}, \tag{19}$$

and the diffusion coefficient characterizing the fluctuations of the cap is

$$\begin{aligned}
D_c &= d^2 \lim_{t \rightarrow \infty} \frac{1}{2} \frac{d}{dt} (\langle k^2 \rangle - \langle k \rangle^2) \\
&= d^2 \lim_{t \rightarrow \infty} \left[\frac{1}{2} \frac{\partial^2}{\partial y^2} \left(\frac{dG(1, y, t)}{dt} \right) + \frac{1}{2} \frac{\partial}{\partial y} \left(\frac{dG(1, y, t)}{dt} \right) \right. \\
&\quad \left. - \left(\frac{\partial G(1, y, t)}{\partial y} \right) \frac{\partial}{\partial y} \left(\frac{dG(1, y, t)}{dt} \right) \right]_{y=1}.
\end{aligned} \tag{20}$$

Phase diagram and average length in the bounded phase

To construct the phase diagram, we first focus on steady-states solutions of Eq. 16, which are such that $dG(x, y, t)/dt = 0$. The obtained equation for $G(x, y)$ involves the following time independent quantities

$$F_0(x) = G(x, 0) = \sum_{n \geq 0} P(n, 0)x^n, \quad (21)$$

$$H_0(y) = G(0, y) = \sum_{k \geq 0} P(0, k)y^k, \quad (22)$$

$$P(0, 0) = F_0(0) = H_0(0) = G(0, 0), \quad (23)$$

which are coupled back to $G(x, y)$.

Progress can be made by considering two particular cases for $x = 1$ and $y = 1$ of this expression for $G(x, y)$. This leads to

$$R - W_T^- = F_0(1) (R + W_D^+) - W_D^- H_0(1) - P(0, 0)W_T^+, \quad (24)$$

$$U - R - W_T^+ = -F_0(1) (R + W_T^+) + W_T^- H_0(1) - P(0, 0)W_T^-. \quad (25)$$

These two equations involve three unknowns $F_0(1)$: the probability that the cap is zero, $H_0(1)$: the probability that the D part of the filament is zero, and $P(0, 0)$: the probability that the filament is in the state of monomers. Note that $P(0, 0) = 0$ in phases of unbounded growth whereas $P(0, 0) > 0$ in the phase of bounded growth.

In the random walk representation of figure 1, the velocity of the random walker in the bulk has components $v_n = (R - W_D^-)d$ along the x axis and $v_k = (U - W_T^+ - R)d$ along the y axis. Depending on the signs of these quantities, four cases emerge. If $v_n > 0$ and $v_k > 0$, both the filament and cap length increase without bound (phase III) which means that $F_0(1) = H_0(1) = P(0, 0) = 0$. If $v_n < 0$ and $v_k < 0$, both the filament and cap length stay bounded (phase I) and $F_0(1) > 0, H_0(1) > 0$ and $P(0, 0) > 0$.

If $v_n > 0$ and $v_k < 0$, the cap length remains constant in time which means $F_0(1) > 0$, but the rest of the filament made of D subunits can be either bounded (for $H_0(1) = P(0, 0) = 0$, which corresponds to phase I) or unbounded (for $H_0(1) = P(0, 0) > 0$ which corresponds to phase IIA). When reporting the condition $H_0(1) = P(0, 0) = 0$ into Eqs. 24-25 and solving for $F_0(1)$, one finds that the phase of bounded growth occurs when $U/(R + W_T^+) < (W_D^+ + W_D^-)/(R + W_D^+)$, and the boundary to the phase of unbounded growth corresponds to replacing the unequal sign by an equal sign.

An alternative way to find this condition is to start from the time dependent evolution equation of $G(x, y, t)$ of Eq. 16 and impose $H_0(y, t) = P(0, 0, t) = 0$. We end up with two coupled dynamical equations for $F_0(x, t)$ and $G(x, y, t)$. The way to obtain the velocity and diffusion coefficient in phase IIA from these equations is explained in details in the appendix of Ref. (11). The result is the expression of v_{IIA} given in Eq. 2, and the expression of D_{IIA} of Eq. 7. As expected, the condition that marks the boundary between phase IIA and phase I corresponds to $v_{IIA} = 0$.

Similarly, if $v_n < 0$ and $v_k > 0$, the length of the region of D subunits at the pointed end remains constant in time, and the region of T subunits can be either bounded (phase I) or unbounded (phase IIB). By either method, one obtains the velocity in the phase IIB given in Eq. 5, and the condition that marks the boundary to phase I, which corresponds to $v_{IIB} = 0$.

In Ref. (11), an explicit expression for the average length in the phase of bounded growth was obtained by a method of cancellation of poles of $G(x, y)$. Unfortunately, this method does not allow us to derive the expression of $G(x, y)$ here, because the rates $W_T^- \neq 0$ and $W_D^- \neq 0$ lead to an additional unknown $H_0(y, t)$ in Eq. 16 which makes the problem much more difficult to solve. For this reason, we could not derive an explicit expression for the average length in this case, and we investigated this quantity only numerically.

B Mean-field equations of the random model

We explain in this appendix how the velocity of the filament in the random model is obtained from a mean-field approach. This appendix is provided mainly for pedagogical reasons, since the solution has already appeared in Ref. (12) and Ref. (26). For simplicity, we focus on the case where growth and shrinking occur only from one end, which we number as the first site $i = 1$. We use the same notations for the rates as in the vectorial model except for the hydrolysis rate, which is denoted r in the random model. For a given configuration, we introduce for each subunit i inside the filament an occupation number τ_i , such that $\tau_i = 1$ if the subunit binds ATP and $\tau_i = 0$ otherwise. In the reference frame associated with the end of the filament, the equations for the average occupation number are

$$\frac{d\langle\tau_1\rangle}{dt} = U(1 - \langle\tau_1\rangle) - W_T\langle\tau_1(1 - \tau_2)\rangle + W_D\langle\tau_2(1 - \tau_1)\rangle - r\langle\tau_1\rangle, \quad (26)$$

$$\begin{aligned} \frac{d\langle\tau_i\rangle}{dt} &= U(\langle\tau_{i-1}(1-\tau_i)\rangle - \langle\tau_i(1-\tau_{i-1})\rangle) + W_T\langle\tau_1[(1-\tau_i)\tau_{i+1} - \tau_i(1-\tau_{i+1})]\rangle \\ &+ W_D\langle(1-\tau_1)[(1-\tau_i)\tau_{i+1} - \tau_i(1-\tau_{i+1})]\rangle - r\langle\tau_i\rangle. \end{aligned} \quad (27)$$

In a mean-field approach, the effect of correlations $\langle\tau_i\tau_j\rangle$ are neglected, *i.e.* these correlations are replaced by $\langle\tau_i\rangle\langle\tau_j\rangle$ (and similarly for averages of product of three occupation numbers). At steady state, the left-hand sides of Eqs. 26-27 are both zero, which leads to recursion relations for the $\langle\tau_i\rangle$. Note that $\langle\tau_i\rangle$ is denoted as a_i in Ref. (26) and as P_i in Ref. (12). We still denote $\langle\tau_1\rangle = q$, since it represents the probability that the terminal unit binds ATP. It is the analog of the parameter defined in Eq. 1 for the vectorial model, which is now a more complicated function of the rates. The recursion relations have a solution of the form for $i \geq 1$,

$$\frac{\langle\tau_{i+1}\rangle}{\langle\tau_i\rangle} = \frac{U - q(W_T + r)}{U - qW_T}. \quad (28)$$

Combining Eqs. 26-28, one obtains the following cubic equation for q

$$\begin{aligned} (W_T + r)(W_T - W_D)q^3 + (UW_D - 2UW_T + W_DW_T + W_Dr) \\ - W_T r - W_T^2 q^2 + U(U - W_D + 2W_T + r)q - U^2 = 0. \end{aligned} \quad (29)$$

$$(29)$$

This cubic equation has three solutions, but only one solution is such that $0 \leq q \leq 1$. The rate of elongation of the filament can be obtained by reporting that solution into

$$v = \frac{d\langle l \rangle}{dt} = [U - W_T q - W_D(1 - q)]d. \quad (31)$$

In figure 7, this velocity v is shown as function of the concentration of free monomers. For low values of r , the velocity of the random and vectorial model are identical, as r is increased the velocity of the random model starts to deviate from the curve of the vectorial model. By imposing the condition $v = 0$, one obtains the phase boundary shown in the solid line in figure 6.

References

1. Howard, J., 2001. Mechanics of Motor Proteins and the Cytoskeleton. Sinauer Associates, Inc., Massachusetts.

2. Fujiwara, I., D. Vavylonis, and T. D. Pollard, 2007. Polymerization kinetics of ADP- and ADP-Pi-actin determined by fluorescence microscopy. *Proc. Natl. Acad. Sci. USA* 104:8827–8832.
3. Phillips, R., J. Kondev, and J. Theriot, 2008. *Physical Biology of the Cell*. Garland Science, first edition.
4. Pieper, U., and A. Wegner, 1996. The end of a polymerizing actin filament contains numerous ATP-Subunit segments that are disconnected by ADP-subunits resulting from ATP Hydrolysis. *Biochem.* 35:4396–4402.
5. Li, X., J. Kierfeld, and R. Lipowsky, 2009. Actin polymerization and depolymerization coupled to cooperative hydrolysis. *Phys. Rev. Lett.* 103:048102.
6. Dimitrov, A., M. Quesnoit, S. Moutel, I. Cantaloube, C. Pous, and F. Perez, 2008. Detection of GTP-tubulin conformation in vivo reveals a role for GTP remnants in microtubule rescues. *Science* 322:1353 – 1356.
7. Vavylonis, D., Q. Yang, and B. O’Shaughnessy, 2005. Actin polymerization kinetics, cap structure, and fluctuations. *Proc. Natl. Acad. Sci. USA*. 102:8543–8548.
8. Bindschadler, M., E. Osborn, C. Dewey, and J. McGrath, 2004. A mechanistic model of the actin cycle. *Biophys. J.* 86:2720–2739.
9. Brooks, F. J., and A. E. Carlsson, 2008. Actin polymerization overshoots and ATP hydrolysis as assayed by pyrene fluorescence . *Biophys. J.* 95:1050–1062.
10. Kueh, H. Y., W. M. Briehner, and T. J. Mitchison, 2008. Dynamic stabilization of actin filaments. *Proc. Natl. Acad. Sci. USA* 105:16531–16536.
11. Ranjith, P., D. Lacoste, K. Mallick, and J.-F. Joanny, 2009. Nonequilibrium self-assembly of a filament coupled to ATP/GTP hydrolysis. *Biophys. J.* 96:2146–2159.
12. Stukalin, E. B., and A. B. Kolomeisky, 2006. ATP hydrolysis stimulates large length fluctuations in single actin filaments. *Biophys. J.* 90:2673–2685.

13. Dogterom, M., and S. Leibler, 1993. Physical aspects of the growth and regulation of microtubule structures. *Phys. Rev. Lett.* 70:1347–1350.
14. Flyvbjerg, H., T. E. Holy, and S. Leibler, 1996. Microtubule dynamics: caps, catastrophes, and coupled hydrolysis. *Phys. Rev. E* 54:5538–5560.
15. Zong, C., T. Lu, T. Shen, and P. G. Wolynes, 2006. Nonequilibrium self-assembly of linear fibers: microscopic treatment of growth, decay, catastrophe and rescue. *Phys. Biol.* 3:83–92.
16. Antal, T., P. L. Krapivsky, S. Redner, M. Mailman, and B. Chakraborty, 2007. Dynamics of an idealized model of microtubule growth and catastrophe. *Phys. Rev. E* 76:041907.
17. Antal, T., P. L. Krapivsky, and S. Redner, 2007. Dynamics of microtubule instabilities. *J. Stat. Mech.* L05004.
18. Sumedha, M. F. Hagan, and B. Chakraborty, 2009. Role of GTP remnants in microtubule dynamics. *arXiv* 0908.1199:1–4.
19. Carlier, M. F., and D. Pantaloni, 1986. Direct evidence for ADP-Pi-F-actin as the major intermediate in ATP-actin polymerization. Rate of dissociation of Pi from actin filaments. *Biochem.* 25:7789–92.
20. Fass, J., C. Pak, J. Bamburg, and A. Mogilner, 2008. Stochastic simulation of actin dynamics reveals the role of annealing and fragmentation. *J. Theor. Biol.* 252:173–183.
21. Hill, T., 1989. Free Energy Transduction and Biochemical Cycle Kinetics. Springer-Verlag, New York.
22. Carlier, M.-F., D. Pantaloni, and E. D. Korn, 1986. The effects of Mg^{2+} at the high-affinity and low-affinity sites on the polymerization of actin and associated ATP hydrolysis. *J. Biol. Chem.* 261:10785–1079.
23. Melki, R., S. Fievez, and M. F. Carlier, 1996. Continuous monitoring of Pi release following nucleotide hydrolysis in actin or tubulin assembly using 2-amino-6-mercapto-7-methylpurine ribonucleoside and purine-nucleoside phosphorylase as an enzyme-linked assay. *Biochem.* 35:1203812045.
24. Pantaloni, D., T. L. Hill, M. F. Carlier, and E. D. Korn, 1985. A model for actin polymerization and the kinetic effects of ATP hydrolysis. *Proc. Natl. Acad. Sci. USA.* 82:7207–7211.

25. Kolomeisky, A. B., and M. E. Fisher, 2001. Force-velocity relation for growing microtubules. *Biophys. J.* 80:149–154.
26. Keiser, T., A. Schiller, and A. Wegner, 1986. Nonlinear increase of elongation rate of actin filaments with actin monomer concentration. *Biochem.* 25:4899–4906.
27. Fujiwara, I., S. Takahashi, H. Tadakuma, T. Funatsu, and S. Ishiwata, 2002. Microscopic analysis of polymerization dynamics with individual actin filaments. *Nat. Cell. Biol.* 4:666–673.
28. Kuhn, J. R., and T. D. Pollard, 2005. Real-time measurements of actin filament polymerization by total internal reflection fluorescence microscopy. *Biophys. J.* 88:1387–1402.
29. Pollard, T. D., 1986. Rate constants for the reactions of ATP- and ADP-actin with the ends of actin filaments. *J. Cell Biol.* 103:2747–2754.
30. T. D. Pollard, R. D. M., L. Blanchoin, 2000. Molecular mechanisms controlling actin filament dynamics in nonmuscle cells. *Annu. Rev. Biophys. Biomol. Struct.* 29:545–576.
31. Chaikin, P. M., and T. Lubensky, 1995. Principles of Condensed Matter Physics. Cambridge University Press.
32. Carlsson, A. E., 2008. Model of reduction of actin polymerization forces by ATP hydrolysis. *Phys. Biol.* 5:036002–036011.

Tables

			References
On rate of T subunits at the barbed end	k_0 ($\mu\text{M}^{-1}\text{s}^{-1}$)	11.6	(1, 12)
Off-rate of T subunits at the barbed end	W_T^+ (s^{-1})	1.4	(1, 12)
Off-rate of T subunits at the pointed end	W_T^- (s^{-1})	0.8	(1, 12)
Off-rate of D subunits at the barbed end	W_D^+ (s^{-1})	7.2	(1, 12)
Off-rate of D subunits at the pointed end	W_D^- (s^{-1})	0.27	(1, 12)
Hydrolysis rate (vectorial model)	R (s^{-1})	0.1-0.3	(12)
Hydrolysis rate (random model)	r (s^{-1})	0.003	(7, 9, 12)

Table 1: Various rates used in the model and corresponding references. The conditions are that of a low ionic strength buffer.

Figure Legends

Figure 1

Schematic diagram representing the addition of subunits with rate U , removal with rates W_T^+ , W_T^- and W_D^+ , and hydrolysis with rate R , which can only occur at the interface between T and D monomers in the vectorial model. Note that two new rates W_T^- and W_D^- have been added as compared to Ref. (11).

Figure 2

Representation of the various possible moves for actin dynamics. (i), (ii) and (iii) depict different cases for vectorial hydrolysis. (iv) and (v) depict cases for random hydrolysis.

Figure 3

Theoretical phase diagram for the vectorial model with two ends in the variables hydrolysis rate R and on-rate U . The line OQ is obtained by setting the cap velocity equal to zero, and the line OP is given by the condition $v_{IIA} = 0$ where v_{IIA} is the velocity in phase IIA calculated in Eq. 2. Similarly, the line OR is given by the condition $v_{IIB} = 0$, where v_{IIB} is the velocity in phase IIB given in Eq. 5.

Figure 4

Filament velocity v versus concentration of free monomers C for the vectorial model with two active ends. (a) Case $R > W_D^-$ for $R = 0.3$. In regions I and IIA, $v = v_{IIA}$, where v_{IIA} is given by Eq. 2. In region III, $v = v_{III}$, where the velocity is that of Eq. 4. (b) Case $R < W_D^-$ for $R = 0.2$. Here $v = v_{IIB}$ where v_{IIB} is given by Eq. 5.

Figure 5

Average length as function of concentration. (filled circles) $W_T^- = 0.8$ and $W_D^- = 0.27$; (open circles) $W_T^- = 0$ and $W_D^- = 0.27$; (open squares) $W_T^- = 0.8$ and $W_D^- = 0$; (filled squares) $W_T^- = 0$ and $W_D^- = 0$. The rates which are not specified here are given in table 1. The black line is $D_{IIA}(c = c_A)/v_{IIA}$

Figure 6

Phase diagram of the random hydrolysis in the coordinate on-rate U versus hydrolysis rate r (per site). The symbols have been obtained from Monte Carlo simulations, while the solid line is the mean-field theory of appendix B. For $r = 0$, we recover the value of U corresponding to the critical concentration of the vectorial model.

Figure 7

Velocity versus free monomer concentration. The squares symbols are experimental data of (22), which were taken from Ref. (32), the solid lines is the velocity for the random model as calculated from the theory presented in appendix B and the plus symbols is the velocity for the vectorial model using rates in table 1 except for $R = 0.12s^{-1}$ and $W_D^+ = 6.7s^{-1}$.

Figure 8

Diffusion coefficient as function of the monomer concentration for the random and vectorial model of hydrolysis. The data points are the prediction for the random model of hydrolysis while the solid lines are the predictions for the vectorial model. The dashed (resp. dash-dotted) vertical line represents the critical concentration for the vectorial (resp. random) model.

Figure 9

(a) and (b) : Total filament length (denoted l , black), and total amount of hydrolyzed subunits (denoted n , grey) as function of time for the case of vectorial hydrolysis (left panel) and random hydrolysis (right panel) (the total concentration of subunits $c_T = 0.7\mu M$; 1 filament in a volume of $10(\mu m)^3$). Note that the point where the two curves meet in the random hydrolysis model occurs much earlier compared to the case of vectorial hydrolysis ($\approx 10000s$). (c) and (d): The variance ($\sigma^2 = \langle l^2 \rangle - \langle l \rangle^2$) as a function of time is plotted for the vectorial model and random model respectively.

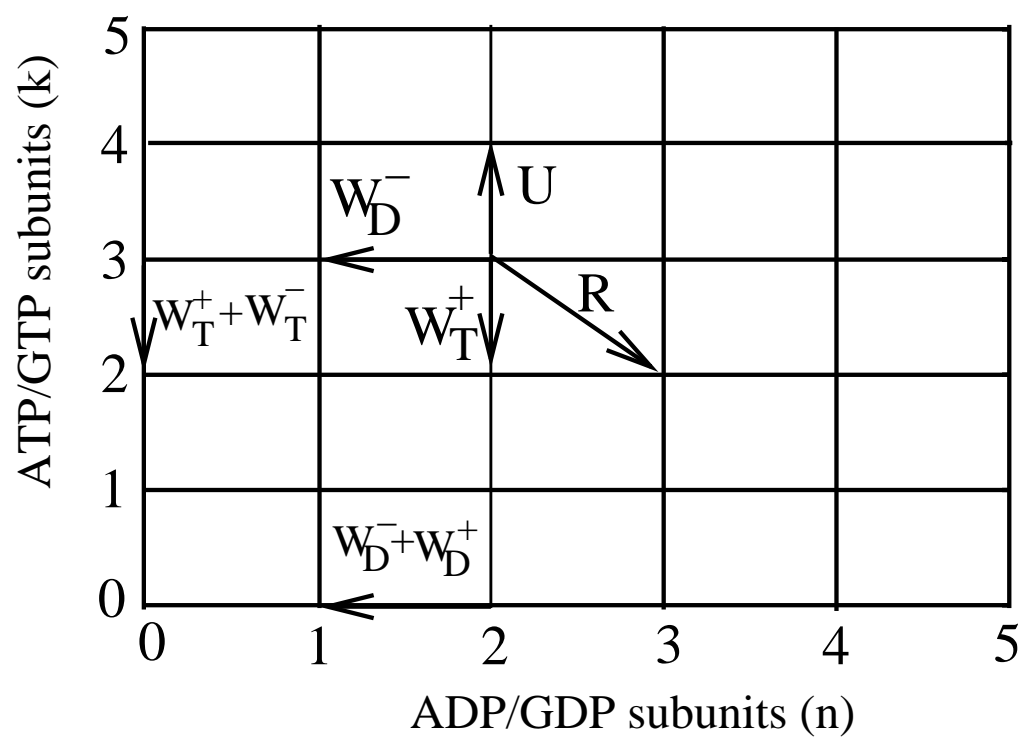


Figure 1:

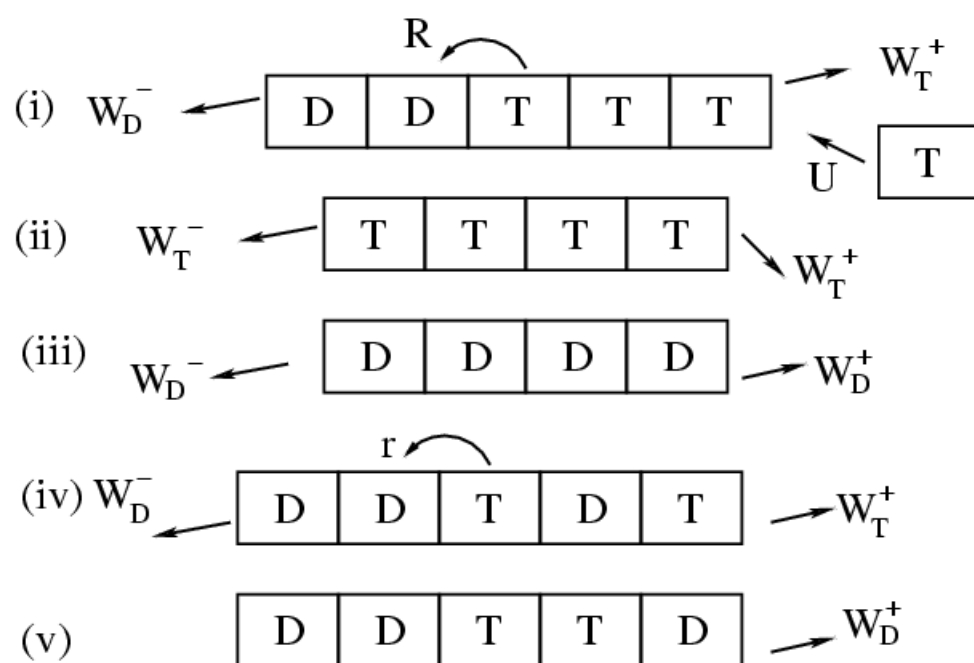


Figure 2:

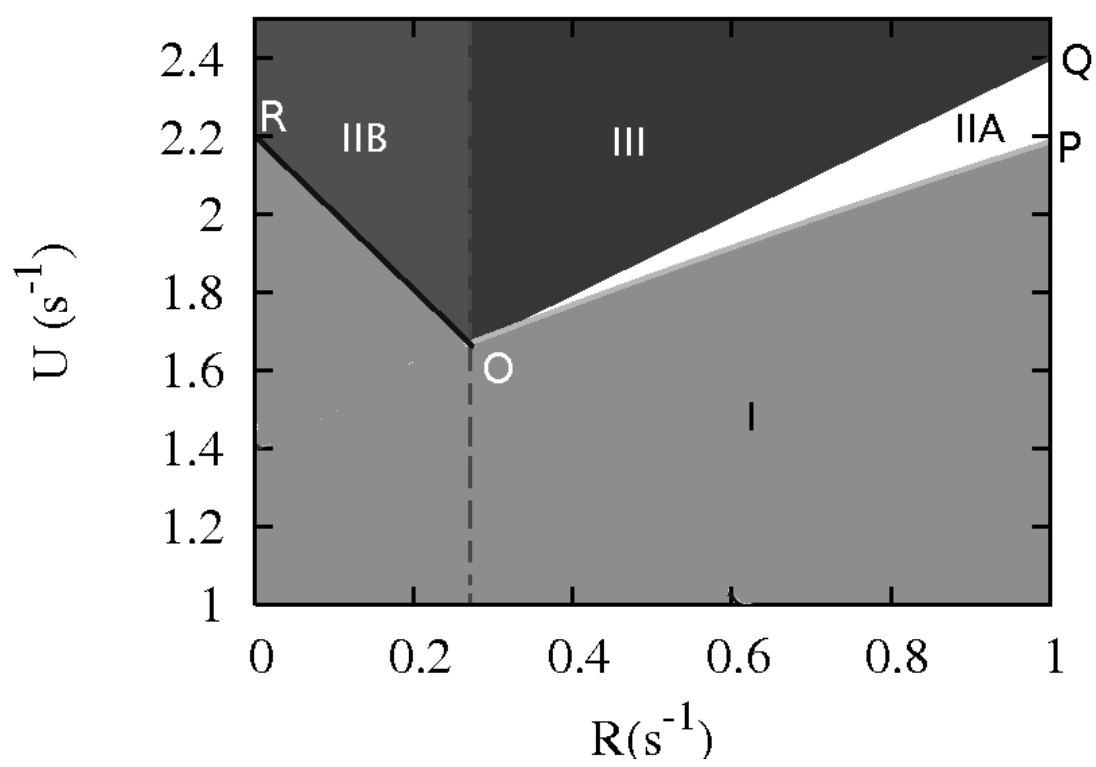


Figure 3:

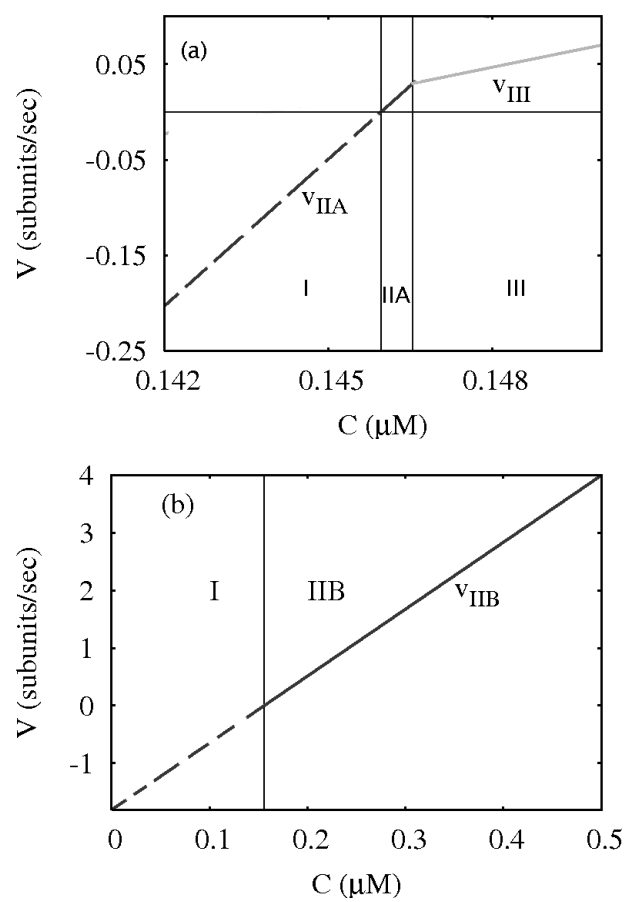


Figure 4:

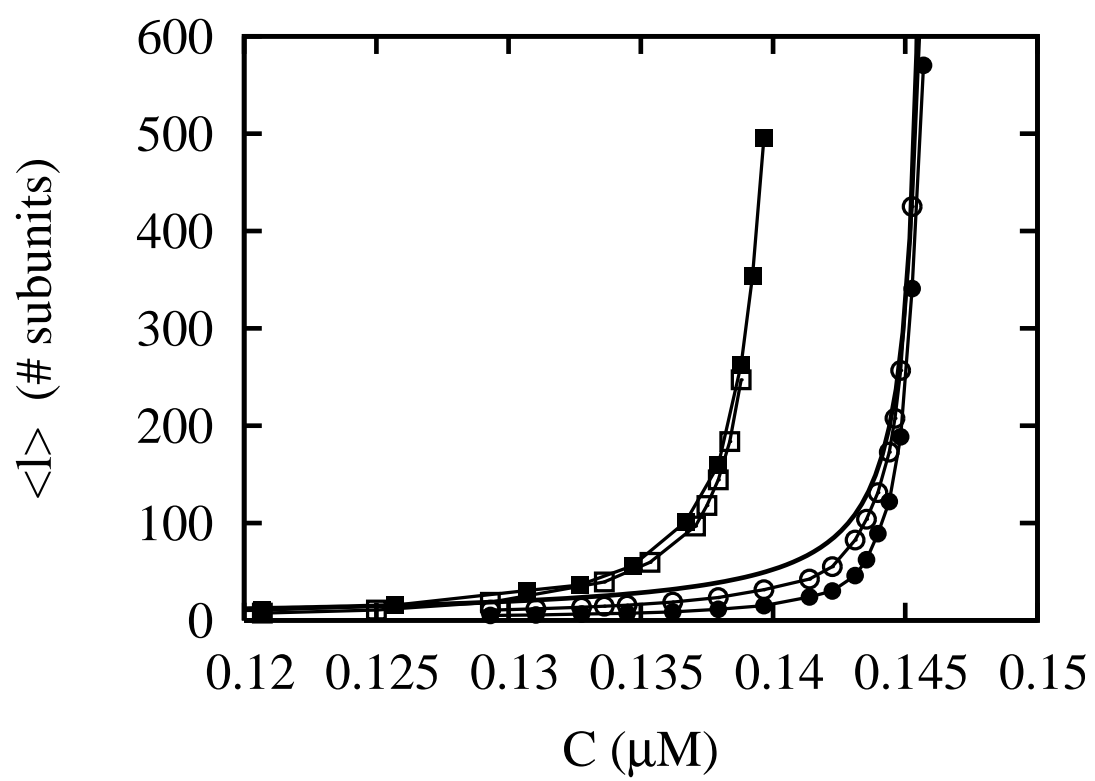


Figure 5:

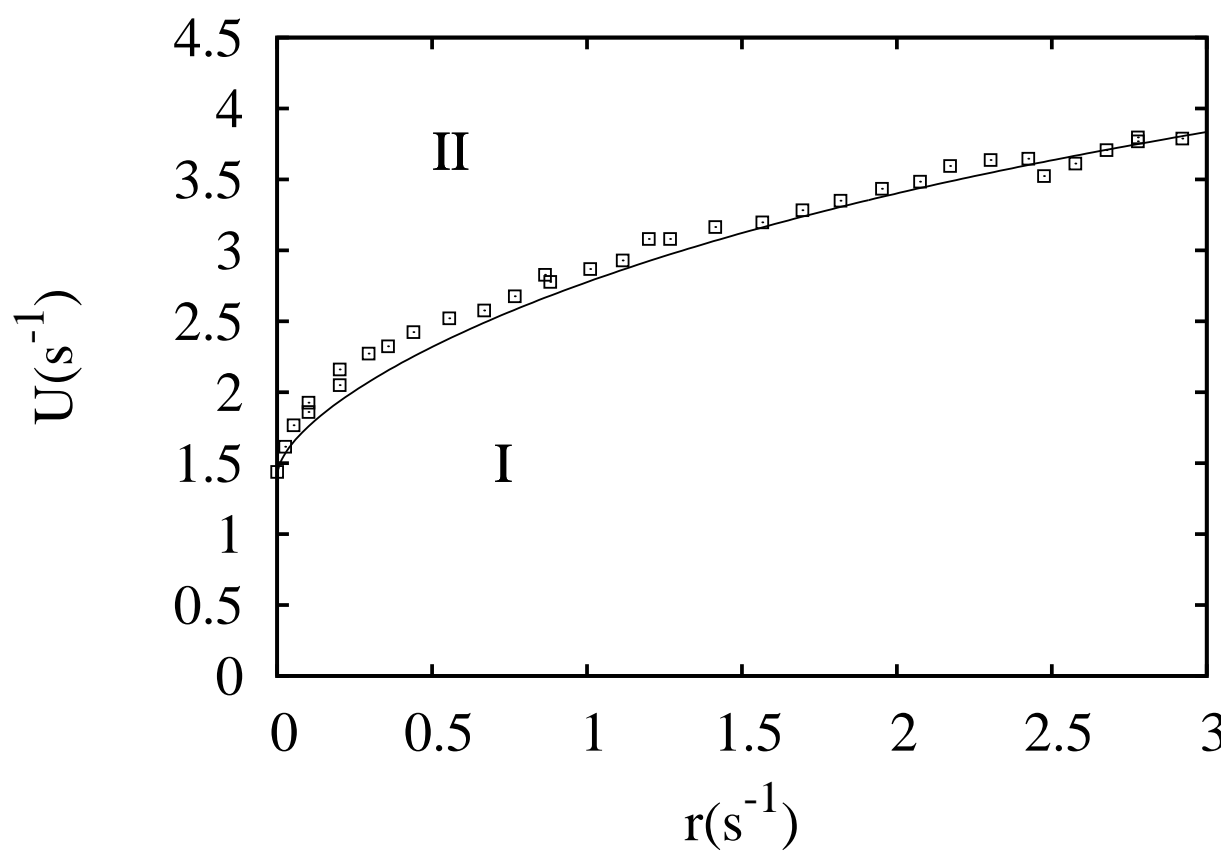


Figure 6:

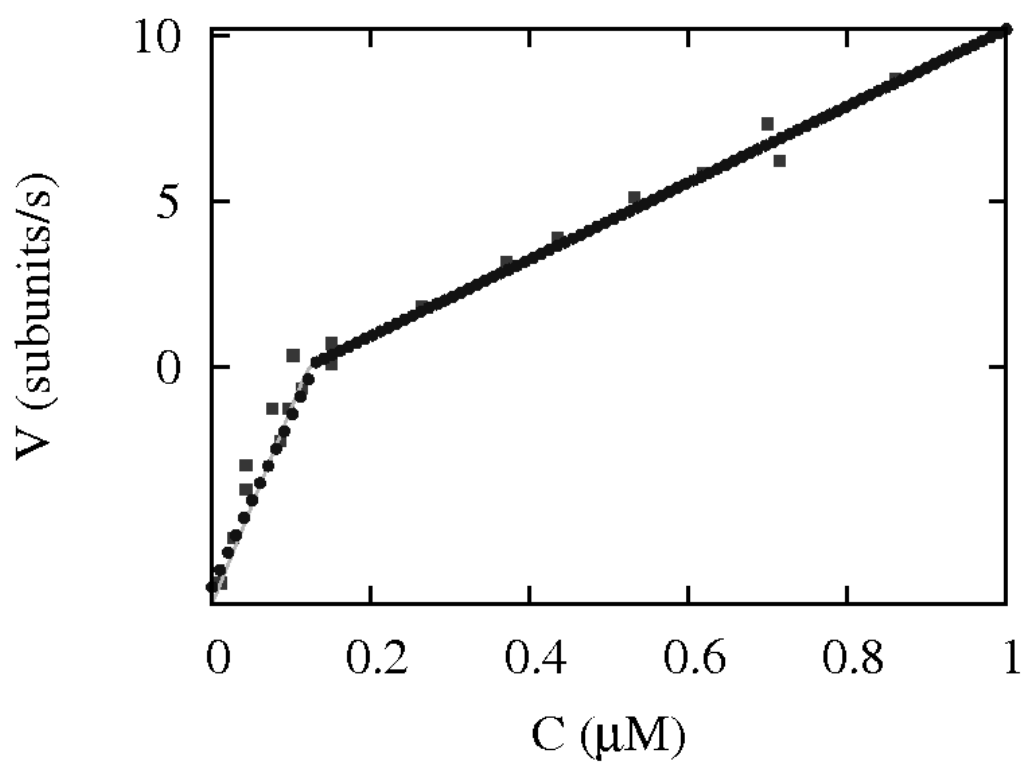


Figure 7:

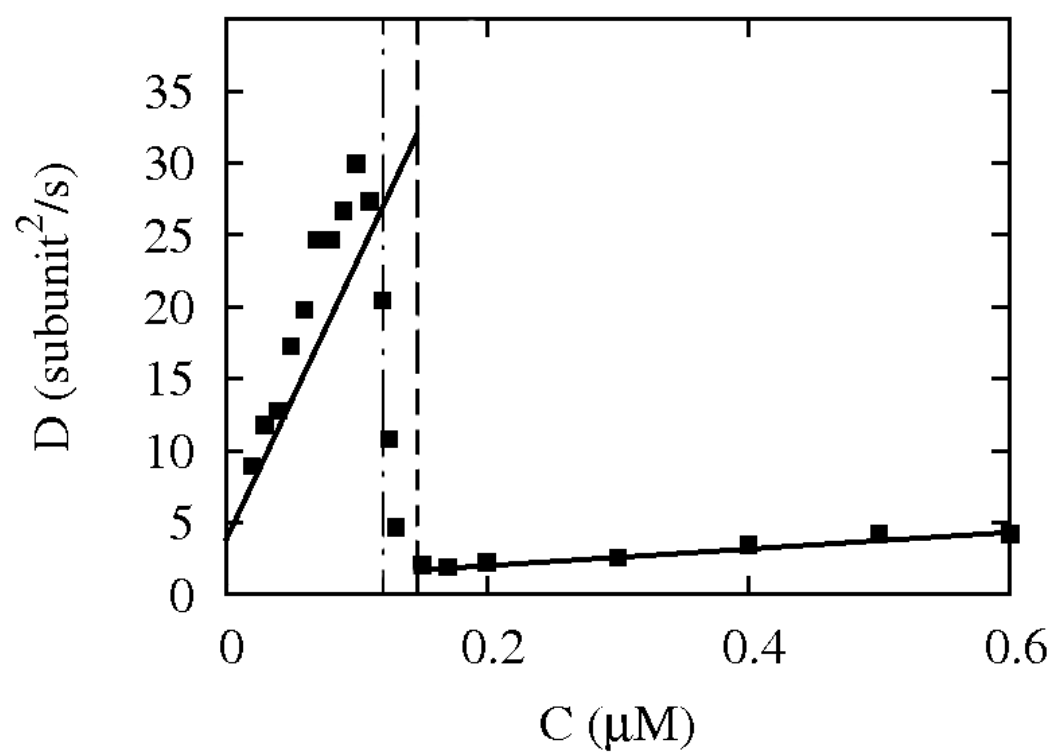


Figure 8:

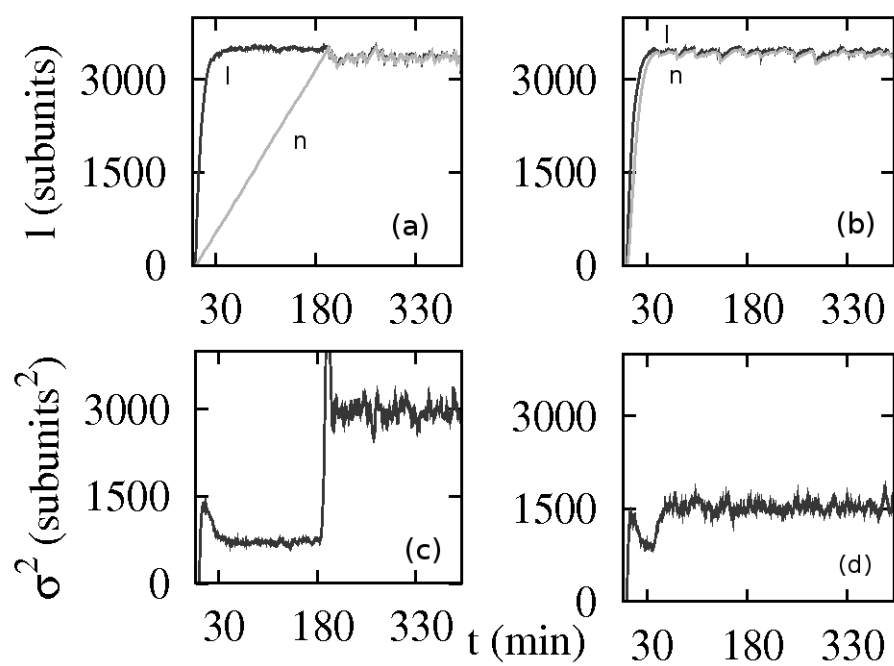


Figure 9: